

Article

# Parameters Extraction of Photovoltaic Models Using an Improved Moth-Flame Optimization

Huawen Sheng, Chunquan Li \*, Hanming Wang, Zeyuan Yan, Yin Xiong, Zhenting Cao and Qianying Kuang

School of Information Engineering, Nanchang University, Nanchang 330029, China; huawensheng@outlook.com (H.S.); wanghanmingcsw@outlook.com (H.W.); zzyilia@outlook.com (Z.Y.); xiongyin@ncu.edu.cn (Y.X.); zhentingcao125@gmail.com (Z.C.); QianYingKuangK@outlook.com (Q.K.)

\* Correspondence: lichunquan@ncu.edu.cn

Received: 1 August 2019; Accepted: 6 September 2019; Published: 13 September 2019



**Abstract:** Photovoltaic (PV) models' parameter extraction with the tested current-voltage values is vital for the optimization, control, and evaluation of the PV systems. To reliably and accurately extract their parameters, this paper presents one improved moths-flames optimization (IMFO) method. In the IMFO, a double flames generation (DFG) strategy is proposed to generate two different types of target flames for guiding the flying of moths. Furthermore, two different update strategies are developed for updating the positions of moths. To greatly balance the exploitation and exploration, we adopt a probability to rationally select one of the two update strategies for each moth at each iteration. The proposed IMFO is used to distinguish the parameter of three test PV models including single diode model (SDM), double diode model (DDM), and PV module model (PMM). The results indicate that, compared with other well-established methods, the proposed IMFO can obtain an extremely promising performance.

**Keywords:** moth-flame optimization; parameter extraction; photovoltaic model; double flames generation (DFG) strategy

## 1. Introduction

Owing to fuel depletion, global warming, and environmental pollution, the renewable energy sources such as wave, tidal, wind, geothermal, and biomass have received more attention in recent years [1–4]. Solar energy is considered as an extremely promising renewable energy source owing to its usability and cleanliness [5–7]. Furthermore, solar energy is also widely adopted to generate power via photovoltaic (PV) systems [8]. However, PV systems are susceptible to external environmental factors such as temperature and global irradiance, affecting the use efficiency of solar energy [9]. Therefore, it is crucial to accurately establish current-voltage models for optimizing and controlling PV systems [10]. The current-voltage models mainly include single diode model (SDM) and double diode model (DDM) [11], which are widely utilized to indicate the connection between current and voltage. The accuracy and reliability of the PV models are primarily determined by their parameters. However, because of unstable operating cases such as faults and aging, the PV models' parameters are generally not available and vary. Thus, developing an effective method to accurately extract these parameters becomes especially critical.

Recently, a large number of algorithms have been proposed for identifying the parameters of PV models. They are mainly divided into the following three categories: analytical [12], deterministic [13], and heuristic methods [14]. The first category methods identify the PV models' parameters via analyzing a set of mathematical formulas [15,16], which accelerates and simplifies the calculation. However, the reliability and accuracy of the solution are poor due to some postulations that need to be made

before the analysis [17,18]. The second category methods are greatly susceptible to initial assumptions and tend to fall into local optimum. In addition, they depend on the model's differentiability or convexity. However, the PV models are usually non-linear and multimodal, resulting in a set of poor solutions when using the second category methods. The third category methods are heuristic methods and can properly overcome the defects of analytical and deterministic methods. Therefore, they have become potential alternatives to PV models' parameters extraction.

Until now, various heuristic algorithms have been proposed for the parameter extraction of the PV models. Reference [14] presents a genetic algorithm (GA) for identifying the SDM parameters of a photovoltaic panel. Reference [19] proposes a new method adopting particle swarm optimization (PSO) with inverse barrier constraint to determine the uncertain parameters of a PV model. Reference [20] applies the artificial bee colony (ABC) to identify the optimal parameters of a silicon solar cell. Reference [21] presents an improved adaptive differential evolution (IADE) algorithm, which utilizes a simple structure based on the feedback of fitness value in the evolutionary process. Reference [22] uses the bird mating optimizer (BMO) to estimate the optimal parameters of silicon solar cell. Reference [23] proposes the chaotic whale optimization algorithm (CWOA), which adopts the chaotic maps to calculate and automatically adapt the internal parameters of the optimization algorithm. Reference [24] presents an improved ant lion optimizer (IALO), which arranges the initial positions of individuals by chaotic sequence to improve the uniformity and ergodicity of population. Reference [25] adopts the bacterial foraging algorithm (BFA) to predict the solar PV characteristics accurately. Reference [26] proposes an improved JAYA (IJAYA) algorithm, in which a self-adaptive weight is proposed to regulate the trend of moving towards the best result, getting out of the worst result at distinct search stages. Reference [27] uses a teaching learning-based optimization (TLBO) algorithm to extract all five parameters of a solar cell. Reference [28] proposes flower pollination algorithm (FPA) to extract the optimal parameters of different PV models.

Furthermore, as a population-based heuristic algorithm, MFO [29] is inspired by moths' behaviors and acquires great performance when solving non-convex and multimodal optimization problems. In MFO, each of the moths represents a solution for problems. Specifically, the algorithm's most striking feature is that each moth has its own flame and flies toward the flame in a spiral curve. Consequently, the flight curves of the moths are always oriented at a fixed angle to the remote target flames, known as the transverse orientation. In MFO, the flames' number is gradually decreased with the iterations' number raising, which allows MFO to obtain fast convergence speed. Note that reference [29] demonstrates MFO's excellent optimization performance in relation to other well-known methods such as GA [18], FPA [28], and PSO [19]. Besides, MFO has been commonly applied to various PV-related practical problems. In reference [30], MFO is utilized to estimate parameters of the three diode models for multi-crystalline solar cells/modules. In reference [31], MFO is used for PV MPPT and partial shading problem. In reference [32], MFO is applied for AI-based MPPT that is used for partial-shaded grid-connected PV plant.

Nevertheless, in MFO, the fast information exchanges among moths are produced owing to all the moths flying toward their best target flames. Once the global optimal value is close to the local optimum, the moths can easily fall into the local optimum of the search area. To overcome the shortcoming of MFO, various MFO variants have been proposed. Reference [33] presents a novel opposition-based moths-flames optimization (OMFO) that uses an opposition-based learning strategy in MFO to improve convergence speed. Reference [34] proposes an efficient hybrid algorithm based on water cycle and MFO algorithms (WCMFO), which combines the Levy-flight operator and spiral movement of MFO into the Water Cycle (WC) method to enhance the WC's ability of exploration and exploitation, respectively. Reference [35] presents a moth-flame optimization algorithm based on chaotic crisscross operator (CCMFO) that uses the chaotic operator and crisscross strategy in MFO to enhance the convergence of premature. However, the above MFO variants have no attempts for solving the PV models' parameters extraction problems.

This paper proposes an improved MFO (IMFO) for accurately estimating the parameters of the PV models. In IMFO, a double-flames generation (DFG) strategy is presented to generate two different kinds of target flames for effectively guiding the flying of moths. By adopting corresponding local best moths, a type of flames called local flame (LF) is produced. Another type of flames is called global flame (GF) and is generated by combining all the moths' current personal best positions (pbests). Furthermore, two different update strategies are created for updating the positions of moths, and each moth only adopts one of the two different evolution update strategies at each iteration. To ensure the effective compromise between global exploration and local exploitation, a probability is utilized to rationally select the two different update strategies for each moth. To demonstrate the superior performance of IMFO, we compare the proposed method with eight well-established algorithms on extracting the parameters of three different PV models, i.e., SDM, DDM, and PMM. The experimental results show that IMFO can achieve a highly competitive performance as well as can reliably and accurately extract the parameters of the three different PV models.

The main contributions of our work are as follows:

1. A novel IMFO algorithm is presented to extract the parameters of different PV models. Different from most existing MFO methods, IMFO develops a double-flames generation (DFG) strategy to generate two kinds of high-performance flames. Furthermore, in IMFO, two different update strategies of moths are developed to effectively tackle exploration and exploitation. Besides, a probability is applied to rationally select one of two different update strategies for each moth's update, contributing the efficient compromise between the global exploration and local exploitation.
2. To the best of our knowledge, there are no MFO methods for solving the parameters extraction on the PMM. Specifically, most existing MFO variants such as OMFO and WCMFO have never been used for the parameter extraction on the three PV models including SDM, DDM, and PMM. Although MFO [30] has been used for the DDM, it has never been adopted for the parameter on the SDM or PMM. However, the proposed IMFO fully considers the parameter extraction on the SDM, DDM, and PMM.
3. Comparisons are given between IMFO and eight well-established algorithms on extracting the parameters of three PV models. The results verify that IMFO can achieve better performance than the eight algorithms on the extraction of the three PV models' parameters.
4. The rest of the paper can be arranged as follows. Section 2 introduces the problem formulation of PV models. The original MFO algorithm is illustrated in Section 3. Section 4 gives the detail of the IMFO algorithm. The experimental results and analysis of different PV models are given in Section 5. Furthermore, the discussion is given in Section 6. Finally, the conclusion is displayed in Section 7.

## 2. Formulation of PV Models

The single diode model (SDM), double diode model (DDM), and PV module model (PMM) are generally adopted to indicate the relationship between current and voltage of solar cells and PV systems. In this section, the SDM, the DDM, and the PMM are given as follows. Furthermore, the objective function for extracting the parameters of the three models is described as follows.

### 2.1. Single Diode Model

The SDM has been commonly used to illustrate the static characteristics of solar cells owing to its simple structure and accuracy. As shown in Figure 1a, the SDM is composed of a diode, a current source, a shunt resistor, and a series resistor. Note that the shunt resistor and series resistor are used for indicating leakage current and denoting load current loss, respectively. The output current  $I_o$  of this diode model can be computed as follows:

$$I_o = I_{ph} - I_d - I_{sh} \quad (1)$$

where  $I_{sh}$ ,  $I_d$ , and  $I_{ph}$  represent the shunt resistor current, the diode current, and the photo produced current, respectively;  $I_o$  denotes the calculated output current. The calculation formulas of  $I_d$  and  $I_{sh}$  are shown as follows:

$$I_d = I_{sd} \left[ \exp\left(\frac{q(V_t + I_t R_s)}{mkT}\right) - 1 \right] \tag{2}$$

$$I_{sh} = \frac{I_t R_s + V_t}{R_{sh}} \tag{3}$$

where  $I_{sd}$  indicates the saturation current of the diode;  $I_t$  and  $V_t$  respectively represent the tested output current and voltage;  $R_s$  means the series resistance;  $q$  and  $k$  are the electron charge ( $1.60217646 \times 10^{-19} \text{C}$ ) and Boltzmann constant ( $1.3806503 \times 10^{-23} \text{J/K}$ ), respectively;  $m$  is the ideal factor of diode;  $T$  is the cell temperature (K);  $R_{sh}$  denotes the shunt resistance. Consequently, we can rewrite Formula (1) as follows:

$$I_o = I_{ph} - I_{sd} \left[ \exp\left(\frac{q(V_t + I_t R_s)}{mkT}\right) - 1 \right] - \frac{I_t R_s + V_t}{R_{sh}} \tag{4}$$

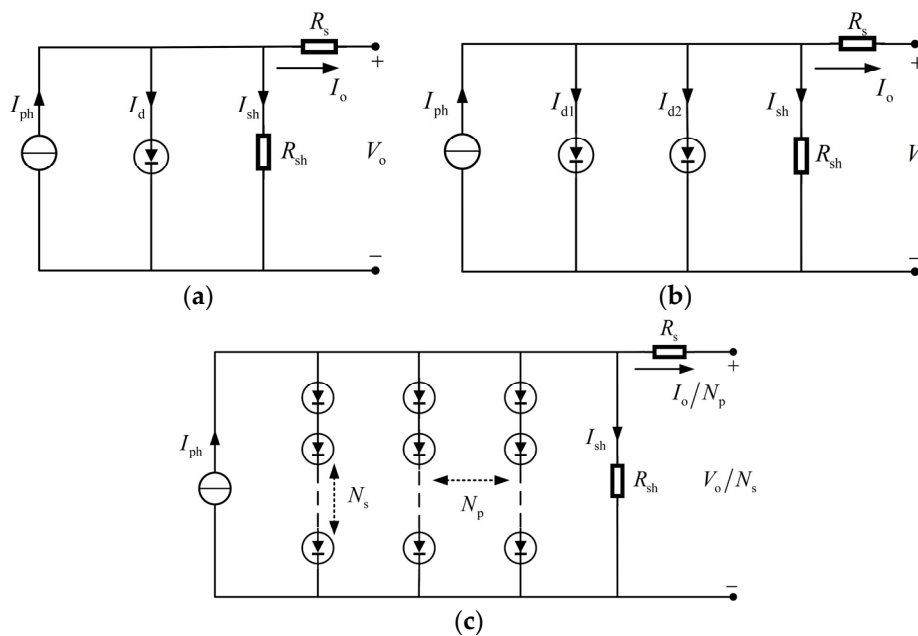


Figure 1. Equivalent circuit diagram of the (a) SDM, (b) DDM, and (c) PMM.

Note that Formula (4) has five undetermined parameters ( $I_{ph}$ ,  $I_{sd}$ ,  $R_s$ ,  $R_{sh}$ , and  $m$ ). Accurate and reliable extraction of the five parameters is important for solar cells, which can be realized by the proposed IMFO algorithms.

### 2.2. Double Diode Model

The DDM has been developed [36,37] due to this fact that the SDM has not considered the influence of composite current loss of the depletion area. As shown in Figure 1b, the DDM contains a current source, two diodes in parallel with a shunt resistance and a resistance in series with the current source. One of the diodes is applied to simulate the charge-recombination current with the non-ideal factors, and the other one is set as the rectifier. The output current  $I_o$  of this model can be acquired as follows:

$$I_o = I_{ph} - I_{d1} - I_{d2} - I_{sh}$$

$$= I_{ph} - I_{sd1} \left[ \exp\left(\frac{q(V_t + I_t R_s)}{m_1 kT}\right) - 1 \right] - I_{sd2} \left[ \exp\left(\frac{q(V_t + I_t R_s)}{m_2 kT}\right) - 1 \right] - \frac{I_t R_s + V_t}{R_{sh}} \tag{5}$$

where  $I_{d1}$  and  $m_1$  denote the current of diffusion and the ideality factor, respectively;  $m_2$  and  $I_{d2}$  indicate the composite diode ideality factor and saturation current, respectively. Different from the SDM, the DDM includes seven undetermined parameters ( $I_{ph}$ ,  $I_{sd1}$ ,  $I_{sd2}$ ,  $R_s$ ,  $R_{sh}$ ,  $m_1$ , and  $m_2$ ) that need to be accurately extracted.

### 2.3. PV Module Model

The PMM typically embodies multiple solar cells connected in parallel and/or in series. The equivalent circuit diagram of the single diode PMM is presented in Figure 1c. The output current of this model can be calculated by the following Formula (6):

$$I_o = N_p \left\{ I_{ph} - I_{sd} \left[ \exp \left( \frac{q(V_t/N_s + I_t R_s/N_p)}{mkT} \right) - 1 \right] - \frac{I_t R_s/N_p + V_t/N_s}{R_{sh}} \right\} \quad (6)$$

where  $N_s$  and  $N_p$  represent the number of solar cells in series and parallel, respectively. Same as the SDM, PMM also has five undetermined parameters ( $I_{ph}$ ,  $I_{sd}$ ,  $R_s$ ,  $R_{sh}$ , and  $m$ ) to be accurately extracted.

### 2.4. Objective Function

For the extraction problem of the undetermined parameters in PV models, the main task is to explore the undetermined parameter optimal value for narrowing the difference between the calculated and tested current values. The errors on each set of calculated and tested current values of the SDM and DDM can be obtained by the following Formulas (7) and (8), respectively.

$$\begin{cases} f_x(V_t, I_t, X) = I_{ph} - I_{sd} \left[ \exp \left( \frac{q(V_t + I_t R_s)}{mkT} \right) - 1 \right] - \frac{I_t R_s + V_t}{R_{sh}} - I_t \\ X = \{I_{ph}, I_{sd}, R_s, R_{sh}, m\} \end{cases} \quad (7)$$

$$\begin{cases} f_x(V_t, I_t, X) = I_{ph} - I_{sd1} \left[ \exp \left( \frac{q(V_t + I_t R_s)}{m_1 kT} \right) - 1 \right] - I_{sd2} \left[ \exp \left( \frac{q(V_t + I_t R_s)}{m_2 kT} \right) - 1 \right] - \frac{I_t R_s + V_t}{R_{sh}} - I_t \\ X = \{I_{ph}, I_{sd1}, I_{sd2}, R_s, R_{sh}, m_1, m_2\} \end{cases} \quad (8)$$

In this work, to evaluate the entire difference between the calculated and tested current values, the root mean square error (RMSE) is utilized as objective functions as shown in Formula (9), which has been commonly adopted in literature [24,26,27]. Particularly, the smaller the RMSE(X) value, the more accurate the extraction of PV models' parameters.

$$RMSE(X) = \sqrt{\frac{\sum_{x=1}^N f_x(V_t, I_t, X)^2}{N}} \quad (9)$$

where  $N$  denotes the number of tested current values,  $X$  is the decision vector that contains the undetermined parameters to be estimated.

## 3. Moth-Flame Optimization Algorithm

As a novel population-based heuristic algorithm, MFO is proposed by Mirjalili in 2015 [29]. The algorithm mainly contains two mechanisms: flame generation mechanism and the spiral flight search mechanism.

### 3.1. Flame Generation Mechanism

In MFO, the whole moth swarm's population size and the individual dimensional size are set as  $N$  and  $D$ , respectively. The whole moth swarm can be expressed as the following matrix  $AM$ :

$$AM = \begin{bmatrix} AM_1 \\ AM_2 \\ \vdots \\ AM_N \end{bmatrix} = \begin{bmatrix} am_{11} & am_{12} & \cdots & \cdots & am_{1D} \\ am_{21} & am_{22} & \cdots & \cdots & am_{2D} \\ \vdots & \vdots & \vdots & \vdots & \vdots \\ am_{N1} & am_{N2} & \cdots & \cdots & am_{ND} \end{bmatrix} \quad (10)$$

where  $AM_i = [am_{i1}, am_{i2}, \dots, am_{iD}]$  represents the state of the  $i$ -th moth,  $i \in \{1, 2, \dots, N\}$ , and  $am_{id}$  indicates the  $d$ -th dimensional position of  $i$ -th moth,  $d \in \{1, 2, \dots, D\}$ . When MFO is applied for the estimating a PV model's parameters, each dimension of  $AM_i = [am_{i1}, am_{i2}, \dots, am_{iD}]$  corresponds to a set of extracted parameters of the PV model;  $D$  stands for the number of the estimated parameters. For example, for the SDM with its five estimated parameters, each  $AM_i$ ,  $i \in \{1, 2, \dots, N\}$  has five dimensions, written as  $AM_i = [am_{i1}, am_{i2}, \dots, am_{i5}]$ ;  $am_{i1}$ ,  $am_{i2}$ ,  $am_{i3}$ ,  $am_{i4}$ , and  $am_{i5}$  represent five estimated parameters  $I_{ph}$ ,  $I_{sd}$ ,  $R_s$ ,  $R_{sh}$ , and  $m$ , respectively.

$F[*]$  denotes the fitness value function. Therefore, for the  $i$ -th moth  $AM_i$ , its fitness value is indicated as  $F[AM_i]$ . Similarly, the fitness value vector of  $AM$  can be represented as follows:

$$F[AM] = \begin{bmatrix} F[AM_1] \\ F[AM_2] \\ \vdots \\ F[AM_N] \end{bmatrix} \quad (11)$$

Similarly, for the estimating a PV model's parameters,  $F[*]$  is defined as objective functions of the PV model.

Due to each moth has its own target flame, the number of the initial flames is equivalent to moths. The matrix  $AF$  is assumed to be the size of initial flames as follows:

$$AF = \begin{bmatrix} AF_1 \\ AF_2 \\ \vdots \\ AF_N \end{bmatrix} = \begin{bmatrix} af_{11} & af_{12} & \cdots & \cdots & af_{1D} \\ af_{21} & af_{22} & \cdots & \cdots & af_{2D} \\ \vdots & \vdots & \vdots & \vdots & \vdots \\ af_{N1} & af_{N2} & \cdots & \cdots & af_{ND} \end{bmatrix} \quad (12)$$

where  $AF_i$  is corresponding to the  $AM_i$ ,  $i \in \{1, 2, \dots, N\}$ .  $D$  and  $N$  are the flames' dimensional number and population size, respectively.

Similarly, for the  $i$ -th flame  $AF_i$ , its fitness value is described as  $F[AF_i]$ . The fitness value vector of  $AF$  is expressed as below:

$$F[AF] = \begin{bmatrix} F[AF_1] \\ F[AF_2] \\ \vdots \\ F[AF_N] \end{bmatrix} \quad (13)$$

The maximum number of iterations and the current number of iterations are set as  $K$  and  $k$ , respectively,  $k \in \{1, 2, \dots, K\}$ . The flame generation mechanism is introduced as follows:

- Step one: when the current iterations' number  $k$  is one, the moths  $\{AM_1, AM_2, \dots, AM_N\}$  are sorted according to their corresponding fitness value  $\{F[AM_1], F[AM_2], \dots, F[AM_N]\}$  from small to large, and the  $i$ -th moth after sorting is set as  $AM_{si}$ ,  $AM_{si} \in \{AM_{s1}, AM_{s2}, \dots, AM_{sN}\}$ . Then, the  $AM_{si}$ ,  $i \in \{1, 2, \dots, N\}$  means the  $i$ -th flame  $AF_i$ . Thus, the  $AF$  and its corresponding fitness value  $F[AF]$  can be initiated based on the sorted  $AM$  and  $F[AM]$ , respectively.

- Step two: when the current number of iterations  $k$  is greater than one but less than or equal to  $K$ . We sort  $AM(k - 1)$  and  $AF(k - 1)$  from small to large according to their corresponding fitness values  $F[AM(k - 1)]$  and  $F[AF(k - 1)]$ . Next, the top  $N$  individuals are selected as new flames  $AF(k)$  from  $AM(k - 1)$  and  $AF(k - 1)$ . The  $F[AM(k - 1)]$  and  $AM(k - 1)$  represent the fitness value vector and the position vector of moths at the  $(k - 1)$ -th iterations, respectively. Similarly, the fitness value vector and position vector of flames at the  $(k - 1)$ -th iterations are  $F[AF(k - 1)]$  and  $AF(k - 1)$ , respectively.

From the above demonstration,  $AF$  denotes the essence of  $AM(k - 1)$  and  $AF(k - 1)$ . Therefore, for the estimating a PV model's parameters, each dimension of  $AF_i = [af_{i1}, af_{i2}, \dots, af_{iD}]$  corresponds to an estimated parameters of the PV model;  $D$  stands for the number of the estimated parameters.

### 3.2. Spiral Flight Search Mechanism

Furthermore, since the moths fly toward their respective target flame in spiral, the spiral flight search mechanism has been developed to simulate the moth's logarithmic spirally flying curve, as below:

$$AM_i(k + 1) = \begin{cases} D_i \cdot e^{bt} \cdot \cos(2\pi t) + AF_i(k), & i \leq F_{nu} \\ D_i \cdot e^{bt} \cdot \cos(2\pi t) + AF_{F_{nu}}(k), & i > F_{nu} \end{cases} \quad (14)$$

where  $AM_i(k + 1)$  indicates the position of the  $i$ -th moth  $AM_i$  after renewing,  $i \in \{1, 2, \dots, N\}$ ;  $D_i = |AF_i - AM_i|$  denotes the distance between the  $i$ -th flame  $AF_i$  and the  $AM_i$ ;  $b$  is a constant for the logarithmic spiral shape;  $t$  is a random number of  $[-1, 1]$ , which denotes the distance between the next position of the moth and the flame ( $t = -1$  is the smallest distance between  $AM_i$  and  $AF_i$ , and  $t = 1$  is the farthest between  $AM_i$  and  $AF_i$ ). For diverse  $t$  values, the spirally flying trajectory in one dimension is displayed in Figure 2.

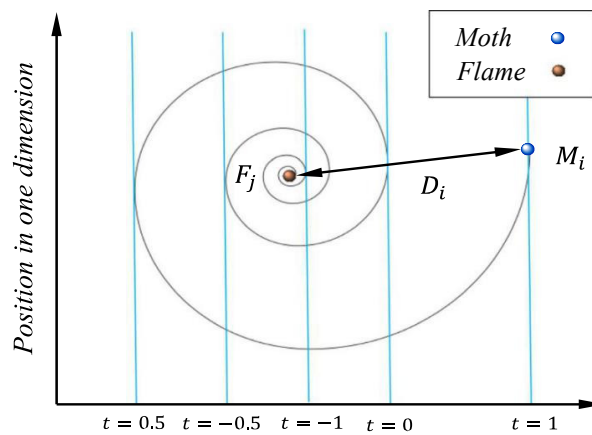


**Figure 2.** Geometric trajectory diagram of flying moth catching flame around logarithmic spiral curve.

$F_{nu}$  is the number of the flames during the iteration process. Note that as the number of iterations increases,  $F_{nu}$  gradually decreases and eventually equals to 1. The process of adaptively reducing the number of flames can be expressed in Formula (15) as below:

$$F_{nu} = \text{round}\left[N - k \times \frac{N - 1}{K}\right] \quad (15)$$

where  $N$  and  $K$  are the maximum number of flames and iterations, respectively;  $k$  denotes the current iterative number. Besides,  $\text{round}[x^*]$  is the function that can make  $x^*$  be rounded to its nearest integer. Note that with  $k = 0$ ,  $F_{nu} = N$ ; when  $k = K$ ,  $F_{nu} = 1$  denotes that moths utilize the best flame to update their own positions at the last iteration in Formula (14).

In general, the flames surrounded by their corresponding moths can be randomly distributed in the search area. Consequently, the MFO can obtain the good balance between the local exploitation and the global exploration [29].

#### 4. Improve Moth-Flame Optimization Algorithm

In the original MFO [29], the moths always flying towards their corresponding best target flames, resulting in the fast communication between moths. Therefore, the moths are easily trapped into local optimum when facing complex multi-modal problems. To address this problem, this paper develops an improved MFO (IMFO) algorithm. In the IMFO, we propose a double-flames generation (DFG) strategy to generate two different types of target flames for guiding moths flying. One type of flames is named local flame (LF), which can be created by dividing the entire swarm into several sub-swarms and then select the local best moths in a corresponding sub-swarm; another one is called global flame (GF) that is generated by combining all the moths' current personal best positions (pbests). Moreover, two different update strategies are developed for updating the positions of moths; each moth only adopts one of the two update strategies at each iteration. In addition, to ensure a great balance between the exploitation and exploration, we develop a probability to rationally select one of the two update strategies for each moth at each iteration. The above process is detailed below.

##### 4.1. Double Flames Generation Strategy

In this strategy, two types of target flames are produced by adopting different moths' information. The first type of flames is the LFs, which can be generated by the following description:

1. Assume the population size of moths is  $N$ ,  $AM_i$  and  $F[AM_i]$  are the position and the fitness value of  $i$ -th moth, respectively,  $i \in \{1, 2, \dots, N\}$ .
2. Divide all the moths in the entire swarm into  $m$  sub-swarms, and each sub-swarm has  $n$  moths. In this case, the  $\alpha$ -th sub-swarm is composed of from number  $(\alpha - 1) \times n + 1$  to number  $\alpha \times n$ ,  $\alpha \in \{1, 2, \dots, m\}$ .
3. According to the moths' fitness values, the best moth of each sub-swarm is select as  $LF_\alpha$ , which denotes the LF of the  $\alpha$ -th sub-swarm.

The second type is GF, which is generated by combining all the moths' pbests. The calculation formula of GF is displayed in Formula (16), we can see from the formula that the GF carries the information about all moths.

$$GF = \frac{1}{N} \sum_{i=1}^N \text{pbest}_i \quad (16)$$

##### 4.2. Update Formulas

Furthermore, two different update strategies are created for generating new moths. Particularly, the two update strategies correspond to two types of flames, respectively as follows:

$$AM_i(k+1) = |LF_\alpha(k) - AM_i(k)| \times e^{bt} \times \cos(2\pi t) + LF_\alpha(k) \quad (\phi > P) \quad (17)$$

$$AM_i(k+1) = |GF(k) - AM_i(k)| \times e^{bt} \times \cos(2\pi t) + GF(k) \quad (\phi \leq P) \quad (18)$$

where  $AM_i(k+1)$  and  $AM_i(k)$  respectively represent the updated position of the  $i$ -th moth at the  $k$ -th and  $(k+1)$ -th iteration,  $i \in \{1, 2, \dots, N\}$ ;  $b$  indicates a constant for the logarithmic spiral shape;  $LF_\alpha(k)$  and  $GF(k)$  denote two type of flames;  $t$  is a number that randomly distributed in the interval of  $[-1,1]$ .

From the Formula (17), we can observe that as the local best flame in the  $\alpha$ -th sub-swarm,  $\alpha \in \{1, 2, \dots, m\}$ ,  $LF_\alpha(k)$  can effectively guide its corresponding moth  $AM_i(k)$  to perform the local search and explore a new potential place in the solution area. On the other hand, we can see from the Formula (18) that the moths in the entire swarm can fly towards  $GF(k)$  for improving the accuracy of solutions. Particularly, instead of using the best flame, Formula (18) adopts  $GF(k)$ , namely the average value of all the moths' pbests to avoid the fast communication between moths and improve the premature of the moths. In general, the two different update strategies make moths obtain the promising compromise between global exploration and local exploitation.

In addition, we develop a probability to rationally select one of the above two update strategies at each iteration. Specifically, a random number  $\phi$  distributed in  $[0,1]$  is created during each iterative process. If the value of  $\phi$  is larger than  $P$ , the Formula (17) can be selected to update the  $i$ -th moth  $AM_i$ ; otherwise, the Formula (18) be done for updating the  $AM_i$ . Therefore, it is significant to acquire a suitable  $P$  value for balancing the exploitation and exploration abilities. The setting of  $P$  value is displayed in Section 6.

#### 4.3. Process of IMFO

The pseudo code of IMFO is expressed in the Algorithm 1, where  $k$  denotes the number of the current iteration;  $LF_\alpha$  denotes the local best flame of the  $\alpha$ -th sub-swarm,  $\alpha \in \{1, 2, \dots, m\}$ , where  $m$  indicates the number of sub-swarms. It can be seen from the Algorithm 1 that the complexity of IMFO is comparable to the original MFO. Moreover, the flow chart of IMFO is described in Figure 3, where the DFG strategy with two different update strategies are adopted to seek the best solution in the search space.

---

#### Algorithm 1: IMFO

---

```

1: /*Initialization*/
2: Initialize the position  $AM_i$  of moths,  $i \in \{1, 2, \dots, N\}$ ;
3: Calculate the fitness value  $F[AM_i]$  of moths, initialize the  $pbest_i, gbest$ ;
4: /* DFG strategy*/
5:  $k = 1$ ;
6: for  $\alpha = 1$  to  $m$  do
7: subswarm $_\alpha = [AM_{(\alpha-1)*n+1}, AM_{(\alpha-1)*n+2}, \dots, AM_{\alpha*n}]$ ;
8: Select the best moth of sub - swarm $_\alpha$  as  $LF_\alpha(k)$ ;
9: end for
10: Calculate the  $GF(k)$  with formula (16);
11: while (condition of termination not met) do
12:  $k = k + 1$ ;
13: for  $i = 1$  to  $N$  do
14: Create a random number  $\phi$ ;
15: if  $\phi > P$ 
16: Update the  $AM_i(k)$  with formula (17);
17: else
18: Update the  $AM_i(k)$  with formula (18);
19: end if
20: Update the  $pbest_i, LF_\alpha, GF, gbest, i \in \{1, 2, \dots, N\}$ ;
21: end for
22: end while

```

---

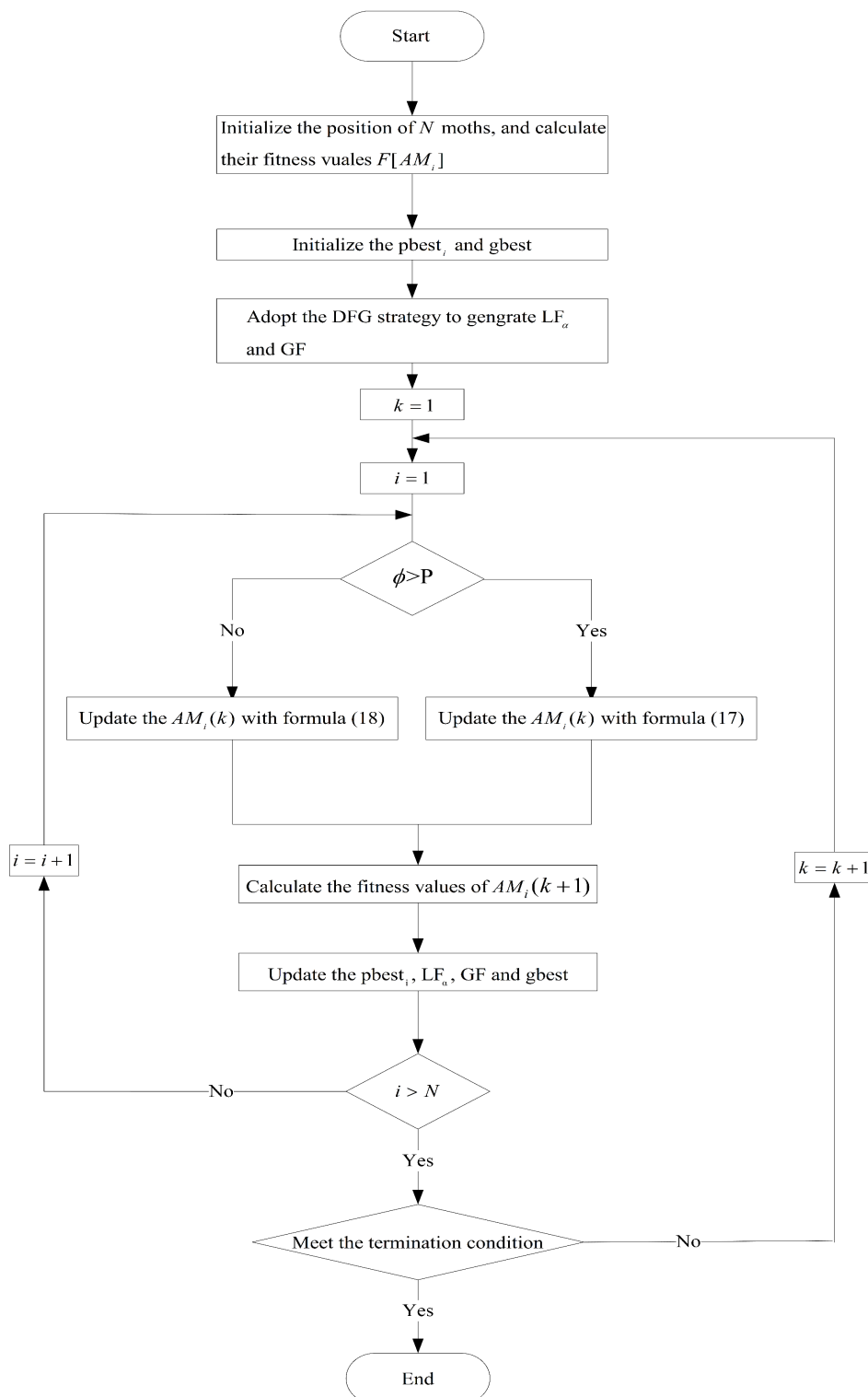


Figure 3. Flow chart of the improved moths-flames optimization (IMFO).

## 5. Results and Analysis

To show the validity of the proposed IMFO method, it is applied to identify the parameters of three different PV models involving the SDM, DDM, and PMM. For the SDM and DDM, reference [18] gives the measured current and voltage values from a 57 mm diameter commercial silicon R.T.C. France silicon solar cell working at a temperature of 33 °C under irradiance of 1000 W/m<sup>2</sup>. Besides, as a PMM, the Photowatt-PWP201 is applied to evaluate the IMFO for identifying the corresponding

parameters [18,38,39]. Particularly, the Photowatt-PWP201 contains 36 silicon cells with series conducting under  $1000 \text{ W/m}^2$  at  $45 \text{ }^\circ\text{C}$ . Considering fair comparison, we utilize the same search upper and lower boundaries [24,26,27] of each parameter of three PV models, as shown in Table 1.

**Table 1.** Parameters boundaries of the three different photovoltaic (PV) models.

Parameter	Single Diode/Double Diode		PV Module	
	Lower Bound	Upper Bound	Lower Bound	Upper Bound
$I_{ph} (A)$	0	1	0	2
$I_{sd1}, I_{sd2} (\mu A)$	0	1	0	50
$R_S (\Omega)$	0	0.5	0	2
$R_{sh} (\Omega)$	0	100	0	2000
$m, m_1, m_2$	1	2	1	50

To indicate the excellent performance of the IMFO method, it has been compared with eight well-established and competitive methods. These compared methods were the basis MFO [30], opposition-based MFO method (OMFO) [33], hybrid water cycle–moth–flame optimization method (WCMFO) [34], brain storm optimization method (BSO) [40], comprehensive learning PSO (CLPSO) method [41], artificial bee colony (ABC) method [20], sine cosine algorithm (SCA) [42], and improved JAYA (IJAYA) method [26]. All the compared methods were independently conducted 30 times on each PV model. For each running, the maximum number of evaluations for the compared methods is set to 50,000. Table A1 of Appendix A shows the parameter settings of the comparison methods. Note that in the IMFO, the population size of moths is set as 100, and the number of sub-swarms and  $P$  are set as four and 0.4, respectively. Moreover, the accuracy of the nine compared methods were illustrated by comparing the best values in their RMSE. Also, their robustness and convergence speed were evaluated through the analysis of data results and convergence curves.

### 5.1. Results on the Single Diode Model

For the SDM, RMSE and the estimated five parameters values are shown in Table 2, where we highlight the overall best and the second best RMSE values in gray boldface and boldface, respectively. Interestingly, both the IMFO and WCMFO achieve the best RMSE value ( $9.8602 \times 10^{-4}$ ) among the nine algorithms; besides, the IJAYA acquires second best RMSE value ( $9.8606 \times 10^{-4}$ ), followed by ABC, CLPSO, MFO, OMFO, BSO, and SCA. RMSE is applied to denote the accuracy of experimental results because of the information of the accurate values of the parameters is not available. Although the gap between the best and second best RMSE values is extremely subtle, it is important to decrease the difference between the true and estimated parameter values in objective function. Because the smaller of objective value RMSE, the more accurate the estimated parameters. Moreover, the extracted best parameters from IMFO are employed to plot  $I$ - $V$  and  $P$ - $V$  curves. This further demonstrates the accuracy of the extracted parameters on SDM. From Figure A1 of Appendix A, we can see that the measured and simulated current and voltage values acquired by IMFO are extremely consistent over the entire voltage range. In addition, the individual absolute errors (IAE) between the simulated and measured current values are displayed in Table A2 of Appendix A. Note that compared with  $2.5 \times 10^{-3}$ , all the IAE values are smaller, demonstrating the preciseness of the extracted parameters from IMFO.

**Table 2.** Comparison among different algorithms on the single diode model.

Algorithm	$I_{ph}(A)$	$I_{sd}(\mu A)$	$R_s(\Omega)$	$R_{sh}(\Omega)$	$m$	RMSE
IMFO	0.76078	0.32296	0.03638	53.71456	1.48117	$9.8602 \times 10^{-4}$
MFO	0.76092	0.30105	0.03596	51.81957	1.46935	$9.9496 \times 10^{-4}$
OMFO	1.09171	0.69332	0.06003	93.11915	2.16144	$1.1927 \times 10^{-3}$
WCMFO	0.76078	0.32314	0.03638	53.69502	1.48122	$9.8602 \times 10^{-4}$
BSO	0.76090	0.99996	0.03137	97.35715	1.60455	$2.4551 \times 10^{-3}$
CLPSO	0.76073	0.31629	0.03639	52.31786	1.47910	$9.9455 \times 10^{-4}$
ABC	0.76085	0.33319	0.03623	53.72712	1.48431	$9.9049 \times 10^{-4}$
SCA	0.76503	0.67937	0.03544	50.14796	1.56094	$5.8058 \times 10^{-3}$
IJAYA	0.76077	0.32349	0.03637	53.89245	1.48133	$9.8606 \times 10^{-4}$

Note:  $9.8602 \times 10^{-4}$ : both the IMFO and WCMFO achieve the best RMSE value among the nine algorithms;  $9.8606 \times 10^{-4}$ : the IJAYA acquires second best RMSE value ( $9.8606 \times 10^{-4}$ ), followed by ABC, CLPSO, MFO, OMFO, BSO, and SCA.

### 5.2. Results on the Double Diode Model

For the DDM, the values of seven extracted parameters with the comparison results of RMSE are presented in Table 3. It can be seen that the proposed IMFO obtain the best RMSE result ( $9.8252 \times 10^{-4}$ ) among the nine methods; the second best RMSE result ( $9.8371 \times 10^{-4}$ ) is achieved by WCMFO. Besides, the  $I$ - $V$  and  $P$ - $V$  curves are rebuilt in Figure A2 through using the best model that estimated by IMFO. Furthermore, via using IMFO, we can obtain IAE values listed in Table A3 of Appendix A, where each of all the IAE values is also smaller than  $2.5 \times 10^{-3}$ . In addition, we can see from the Figure A2 of Appendix A that the measured and simulated current and voltage values obtained by IMFO are highly in coincidence. Therefore, IMFO can extract the parameters of DDM with high accuracy.

**Table 3.** Comparison among different algorithms on the double diode model.

Algorithm	$I_{ph}(A)$	$I_{sd1}(\mu A)$	$R_s(\Omega)$	$R_{sh}(\Omega)$	$m_1$	$I_{sd2}(\mu A)$	$m_2$	RMSE
IMFO	0.76078	0.23350	0.03671	55.29970	1.45374	0.68372	2.00000	$9.8252 \times 10^{-4}$
MFO	0.76087	0.15997	0.03699	52.76975	1.43092	0.55840	1.82735	$1.0102 \times 10^{-3}$
OMFO	0.76078	0.01137	0.03644	53.27466	1.46548	0.30651	1.48014	$9.8652 \times 10^{-4}$
WCMFO	0.76078	0.23956	0.03661	55.11475	1.45681	0.44291	1.90457	$9.8371 \times 10^{-4}$
BSO	0.76100	0.00001	0.03134	92.63446	1.14459	0.99843	1.60458	$2.4636 \times 10^{-3}$
CLPSO	0.76066	0.28752	0.03664	55.28951	1.95861	0.26868	1.46524	$9.9224 \times 10^{-4}$
ABC	0.76051	0.24568	0.03641	58.63990	1.46175	0.26266	1.76608	$1.0001 \times 10^{-3}$
SCA	0.76540	0.00000	0.02945	38.07191	1.02508	0.95693	1.60284	$9.2482 \times 10^{-3}$
IJAYA	0.76077	0.64791	0.03675	54.86248	1.98667	0.22965	1.45222	$9.8380 \times 10^{-4}$

Note:  $9.8252 \times 10^{-4}$ : It can be seen that the proposed IMFO obtain the best RMSE result among the nine methods; the second best RMSE result ( $9.8371 \times 10^{-4}$ ) is achieved by WCMFO.

### 5.3. Results on the PV Module Model

For the PMM, it has five parameters that need to be estimated. Table 4 presents the best RMSE and the five extracted parameters values for each of the nine compared methods on 30 tests. From the Table 4, we can see that IMFO achieves the best RMSE value ( $2.4251 \times 10^{-3}$ ); the IJAYA has the second best RMSE value ( $2.2453 \times 10^{-3}$ ). Furthermore, Figure A3 of Appendix A shows that the  $I$ - $V$  and  $P$ - $V$  curves features of the estimated parameters by IMFO are good in coincidence with the measured values. In addition, Table A4 of Appendix A indicates that each of all the IAE values is smaller than  $4.8 \times 10^{-3}$ . From these results, IMFO can achieve the great accuracy parameters extraction.

**Table 4.** Comparison among different algorithms on the PV module model.

Algorithm	$I_{ph}(A)$	$I_{sd}(\mu A)$	$R_s(\Omega)$	$R_{sh}(\Omega)$	$m$	RMSE
IMFO	1.03052	3.47835	1.20139	980.46728	48.63854	<b><math>2.4251 \times 10^{-3}</math></b>
MFO	1.02807	4.06598	1.19215	1185.52443	49.19573	$2.4576 \times 10^{-3}$
OMFO	1.03062	3.41288	1.20337	961.83398	48.56592	$2.4257 \times 10^{-3}$
WCMFO	1.03039	3.53468	1.19979	1003.12281	48.69988	$2.4255 \times 10^{-3}$
BSO	1.03591	1.18207	1.31645	593.82890	44.80230	$4.7604 \times 10^{-3}$
CLPSO	1.03013	3.62057	1.19763	1043.44361	48.79166	$2.4282 \times 10^{-3}$
ABC	1.03095	3.79242	1.18896	946.21624	48.97719	$2.4660 \times 10^{-3}$
SCA	1.04244	4.68166	1.20422	1204.05479	49.78753	$1.0327 \times 10^{-2}$
IJAYA	1.03047	3.50872	1.20024	987.63650	48.67208	<b><math>2.4253 \times 10^{-3}</math></b>

Note: IMFO achieves the best RMSE value  **$2.4251 \times 10^{-3}$** ; the IJAYA has the second best RMSE value  **$2.4251 \times 10^{-3}$** .

5.4. Statistical Results and Convergence Curves

In this section, IMFO is compared with the other eight methods on the reliability and convergence speed by the convergence curves and statistical results. Table 5 displays the nine algorithms' statistical results over 30 independent tests on each of three PV models, where the minimum (min), mean and standard deviation (SD) values of RMSE represent the accuracy, average preciseness and reliability of the extracted parameters, respectively. Besides, we conduct the Wilcoxon signed-rank examination at 5% significant level [43] to verify the great differences between IMFO and other compared methods. Sign "+" in the Table 5 indicates that the IMFO is greatly superior to its competitors.

**Table 5.** Comparisons on the statistical results of different algorithms for three different PV models.

Model	Algorithm	RMSE				Sig.
		Min	Mean	Max	SD	
Single diode model	IMFO	<b><math>9.8602 \times 10^{-4}</math></b>	<b><math>9.8767 \times 10^{-4}</math></b>	<b><math>9.964110^{-4}</math></b>	<b><math>2.181010^{-6}</math></b>	
	MFO	$9.9496 \times 10^{-4}$	$1.9256 \times 10^{-3}$	$2.584910^{-3}$	$4.925510^{-4}$	+
	OMFO	$1.1927 \times 10^{-3}$	$2.1967 \times 10^{-3}$	$5.836910^{-3}$	$8.52141^{-4}$	+
	WCMFO	<b><math>9.8602 \times 10^{-4}</math></b>	<b><math>1.0122 \times 10^{-3}</math></b>	$1.330510^{-3}$	$7.342310^{-5}$	+
	BSO	$2.4551 \times 10^{-3}$	$2.6986 \times 10^{-3}$	$3.330710^{-3}$	$1.96141^{-4}$	+
	CLPSO	$9.9455 \times 10^{-4}$	$1.0507 \times 10^{-3}$	$1.186510^{-3}$	$4.673010^{-5}$	+
	ABC	$9.9049 \times 10^{-4}$	$1.2951 \times 10^{-3}$	$1.927810^{-3}$	$2.548310^{-4}$	+
	SCA	$5.8058 \times 10^{-3}$	$3.7413 \times 10^{-2}$	$4.863610^{-2}$	$1.302310^{-2}$	+
	IJAYA	<b><math>9.8606 \times 10^{-4}</math></b>	$1.0261 \times 10^{-3}$	<b><math>1.122310^{-3}</math></b>	<b><math>4.160910^{-5}</math></b>	+
Double diode model	IMFO	<b><math>9.8252 \times 10^{-4}</math></b>	<b><math>9.9737 \times 10^{-4}</math></b>	<b><math>1.140910^{-3}</math></b>	<b><math>3.293910^{-5}</math></b>	
	MFO	$1.0102 \times 10^{-3}$	$3.4150 \times 10^{-3}$	$3.521510^{-2}$	$5.689710^{-3}$	+
	OMFO	$9.8652 \times 10^{-4}$	$2.1677 \times 10^{-3}$	$3.727710^{-3}$	$7.301810^{-4}$	+
	WCMFO	<b><math>9.8371 \times 10^{-4}</math></b>	$1.1449 \times 10^{-3}$	$2.264810^{-3}$	$3.080910^{-4}$	+
	BSO	$2.4636 \times 10^{-3}$	$2.8700 \times 10^{-3}$	$4.090610^{-3}$	$3.704510^{-4}$	+
	CLPSO	$9.9224 \times 10^{-4}$	$1.0522 \times 10^{-3}$	<b><math>1.146210^{-3}</math></b>	<b><math>4.314110^{-5}</math></b>	+
	ABC	$1.0001 \times 10^{-3}$	$1.0936 \times 10^{-3}$	$1.289610^{-3}$	$7.411110^{-5}$	+
	SCA	$9.2482 \times 10^{-3}$	$4.2445 \times 10^{-3}$	$2.228610^{-1}$	$3.624810^{-2}$	+
	IJAYA	$9.8380 \times 10^{-4}$	<b><math>1.0240 \times 10^{-3}</math></b>	$1.350710^{-3}$	$8.564710^{-5}$	+
PV module model	IMFO	<b><math>2.4251 \times 10^{-3}</math></b>	<b><math>2.4294 \times 10^{-3}</math></b>	<b><math>2.500510^{-3}</math></b>	<b><math>1.383110^{-5}</math></b>	
	MFO	$2.4576 \times 10^{-3}$	$2.7962 \times 10^{-3}$	$5.175410^{-3}$	$5.728310^{-4}$	+
	OMFO	$2.4257 \times 10^{-3}$	$2.5901 \times 10^{-3}$	$2.639110^{-3}$	$5.258610^{-5}$	+
	WCMFO	$2.4255 \times 10^{-3}$	$1.1551 \times 10^{-2}$	$2.742510^{-1}$	$4.961610^{-2}$	+
	BSO	$4.7604 \times 10^{-3}$	$2.0011 \times 10^{-1}$	$4.063510^{-1}$	$1.051610^{-1}$	+
	CLPSO	$2.4282 \times 10^{-3}$	$2.4527 \times 10^{-3}$	$2.527710^{-3}$	$2.382810^{-5}$	+
	ABC	$2.4660 \times 10^{-3}$	$2.6049 \times 10^{-3}$	$2.759510^{-3}$	$5.996210^{-5}$	+
	SCA	$1.0327 \times 10^{-2}$	$1.2834 \times 10^{-1}$	$2.743310^{-1}$	$1.074010^{-1}$	+
	IJAYA	<b><math>2.4253 \times 10^{-3}</math></b>	<b><math>2.4404 \times 10^{-3}</math></b>	<b><math>2.502610^{-3}</math></b>	<b><math>1.976710^{-5}</math></b>	+

We can clearly see from the Table 5 that the IMFO algorithm achieves the more outstanding performance than other eight algorithms on the reliability and average accuracy of the three models. For the SDM, WCMFO and IJAYA obtain the second-best average accuracy and reliability, respectively. For the DDM, the second-best reliability and average accuracy are acquired by IJAYA and CLPSO, respectively. For the PMM, the IJAYA achieves the second-best result both on average accuracy and reliability. Moreover, the results of Wilcoxon signed-rank test from Table 5 demonstrate that IMFO presents the greatly superior to all the compared methods on all the three models. Figure A4 of Appendix A displays the box-plots, indicating the distribution of all the 30 independent runs' results acquired by the nine different methods. Note that the sign “+” in Figure A4 represents the abnormal value during the plotting. The span of the data distributions demonstrates that the superior performance is also obtained by IMFO algorithm.

Furthermore, Figure 4 gives the convergence curves of nine methods, which are plotted by using the average RMSE value on the 30 independent tests. Clearly, IMFO acquired the fastest convergence speed among the nine methods on each of the three PV models.

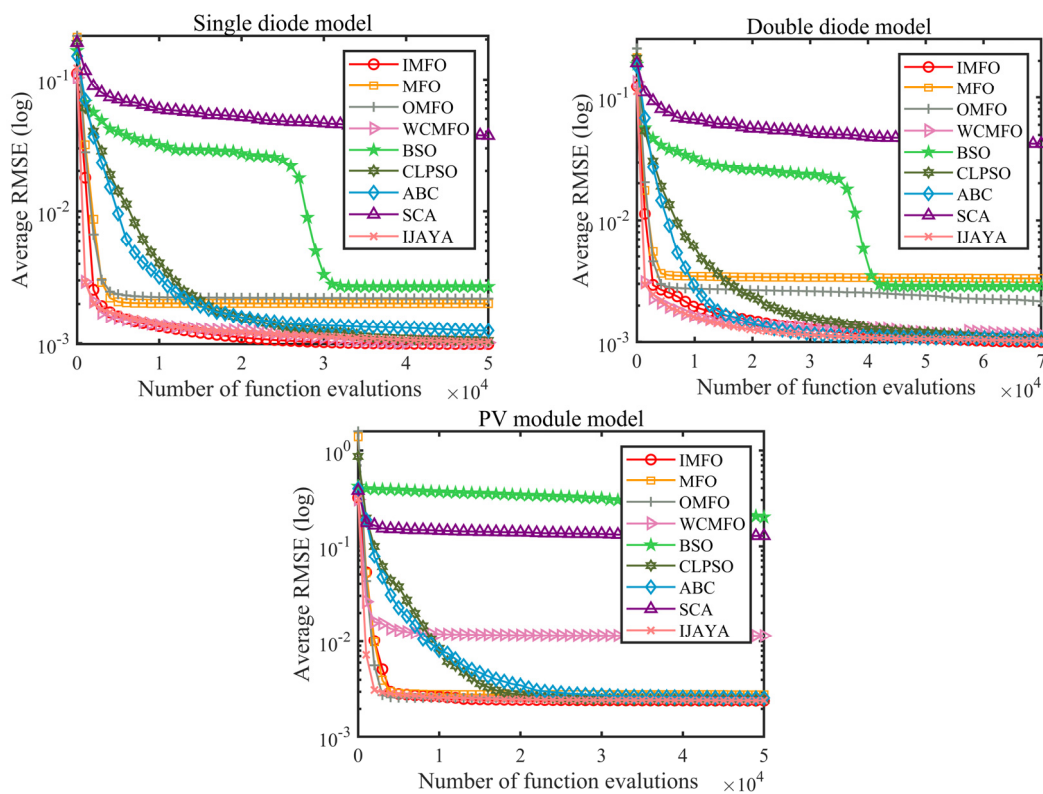


**Figure 4.** Convergence curves of different algorithms for three models.

In general, according to the above comparisons, we can indicate that the IMFO method expresses the superior performance on searching preciseness, reliability and faster convergence performance when extracting the three different PV models' parameters. Besides, IMFO performs the superior and competitive performance in contrast with eight mature heuristic methods.

## 6. Discussion

### 6.1. Discussion of Parameter

In this paper, the parameter  $P$  is used to rationally select one of the two update strategies for each moth at each iteration. Thus, it is significant to set a suitable  $P$  value for balancing the local exploitation and global exploration abilities. In this section, we test the influences of different  $P$  values on IMFO performance through comparing the preciseness and reliability when extracting the parameters of the

three different PV models. The maximum number of evaluations is also set as 50,000 on each running; the population size of the moths and number of sub-swarms are set as 100 and 4, respectively.

We evaluate the IMFO with three different  $P$  values: 0.4, 0.5 and 0.6. In addition, the IMFO with each different  $P$  value is independently conducted 30 times on each model. Table 6 shows that  $P = 0.4$  provides the best values on all the three different PV models according to all criteria. This means that  $P = 0.4$  can obtain the best performance on accuracy and reliability when estimating the three models' parameters.

**Table 6.** Statistical results of root mean square error (RMSE) of IMFO with different settings of  $P$  on the three models.

Model	$P$	RMSE			
		Min	Mean	Max	SD
Single diode model	$P = 0.4$	<b><math>9.8602 \times 10^{-4}</math></b>	<b><math>9.8767 \times 10^{-4}</math></b>	<b><math>9.9641 \times 10^{-4}</math></b>	<b><math>2.1810 \times 10^{-6}</math></b>
	$P = 0.5$	$9.8605 \times 10^{-4}$	<b><math>9.9166 \times 10^{-4}</math></b>	$1.0558 \times 10^{-3}$	<b><math>1.2596 \times 10^{-5}</math></b>
	$P = 0.6$	<b><math>9.8604 \times 10^{-4}</math></b>	$1.0592 \times 10^{-3}$	$1.6218 \times 10^{-3}$	$1.5329 \times 10^{-4}$
Double diode model	$P = 0.4$	<b><math>9.8252 \times 10^{-4}</math></b>	<b><math>9.9737 \times 10^{-4}</math></b>	<b><math>1.1409 \times 10^{-3}</math></b>	<b><math>3.2939 \times 10^{-5}</math></b>
	$P = 0.5$	<b><math>9.8259 \times 10^{-4}</math></b>	<b><math>1.0316 \times 10^{-3}</math></b>	<b><math>1.3051 \times 10^{-3}</math></b>	<b><math>9.3092 \times 10^{-5}</math></b>
	$P = 0.6$	$9.8463 \times 10^{-4}$	$1.1169 \times 10^{-3}$	$1.5621 \times 10^{-3}$	$1.8730 \times 10^{-4}$
PV module model	$P = 0.4$	<b><math>2.4251 \times 10^{-3}</math></b>	<b><math>2.4294 \times 10^{-3}</math></b>	<b><math>2.5005 \times 10^{-3}</math></b>	<b><math>1.3831 \times 10^{-5}</math></b>
	$P = 0.5$	<b><math>2.4251 \times 10^{-3}</math></b>	$2.0553 \times 10^{-2}$	<b><math>2.7425 \times 10^{-1}</math></b>	$6.8963 \times 10^{-2}$
	$P = 0.6$	<b><math>2.4252 \times 10^{-3}</math></b>	<b><math>1.1607 \times 10^{-2}</math></b>	<b><math>2.7425 \times 10^{-1}</math></b>	<b><math>4.9607 \times 10^{-2}</math></b>

## 6.2. Discussion of IMFO

To demonstrate that IMFO can effectively escape the local optimum when solving multimodal problems, we further tested the performance of IMFO, MFO [30], OMFO [33], WCMFO [34], BSO [40], CLPSO [41], ABC [20], SCA [42], and IJAYA [26] on the CEC2017 benchmark suite [44]. Due to the space constraints, the 30 benchmark functions of CEC2017 were listed in Table A5 of the Appendix A. Moreover, according to the characteristics of the 30 benchmark functions, they can be classified into unimodal, multimodal, hybrid, and composition problems. In addition, each function has the same search boundary range  $(-100,100)$  on each dimension. Note that  $F(x^*)$  is the optimal value of each function;  $x^*$  is the best solution corresponding to the optimal value. Here, owing to the limited space, we select F4, F7, and F8 from the multimodal functions, and F12 and F18 from the hybrid functions for evaluating the nine compared algorithms. Each evaluated algorithm was conducted 30 times independently on each of the five selected benchmarks. The mean values (Mean) of the corresponding errors are used as rating criteria. The comparison results of the nine algorithms with 30 dimensions are displayed in Table 7, where we highlight the best and second-best Mean results in gray boldface and boldface, respectively.

From the Table 7, we can see that IMFO achieves the best error means among the nine algorithms on all the five complex functions. Moreover, the indicators of IMFO on the five benchmark functions are all superior to the conventional MFO. For example, IMFO can provide the results of errors' mean values  $5.06$  and  $7.30 \times 10$  on multimodal functions F4 and F7, respectively, which are both close to the optimal error value 0. However, MFO only can obtain the results of errors' mean values  $8.91 \times 10^2$  and  $3.42 \times 10^2$  on multimodal functions F4 and F7, respectively. The above analysis shows that IMFO can find a more promising solution than the MFO of the multimodal problem in the search space. This indicates that MFO is easily trapped into the local optimum when solving complex multimodal problems, however, IMFO can effectively escape the local optimum to find a more promising solution on the multimodal problems.

**Table 7.** Comparisons between IMFO and eight algorithms on five benchmark functions of CEC2017 with 30 dimensions.

Criteria	Algorithm	F4	F7	F8	F12	F18
Mean	IMFO	<b>5.06</b>	<b>7.30 × 10</b>	<b>4.48 × 10</b>	<b>2.16 × 10<sup>4</sup></b>	<b>8.61 × 10<sup>4</sup></b>
	MFO	8.91 × 10 <sup>2</sup>	3.42 × 10 <sup>2</sup>	1.86 × 10 <sup>2</sup>	3.34 × 10 <sup>8</sup>	2.52 × 10 <sup>6</sup>
	OMFO	9.04 × 10	2.28 × 10 <sup>2</sup>	1.17 × 10 <sup>2</sup>	4.86 × 10 <sup>6</sup>	4.17 × 10 <sup>5</sup>
	WCMFO	7.74 × 10	6.63 × 10 <sup>2</sup>	2.09 × 10 <sup>2</sup>	7.12 × 10 <sup>5</sup>	<b>1.52 × 10<sup>5</sup></b>
	BSO	8.86 × 10	3.66 × 10 <sup>2</sup>	1.25 × 10 <sup>2</sup>	1.63 × 10 <sup>6</sup>	1.72 × 10 <sup>5</sup>
	CLPSO	7.03 × 10	<b>8.84 × 10</b>	<b>5.25 × 10</b>	<b>4.27 × 10<sup>5</sup></b>	1.33 × 10 <sup>5</sup>
	ABC	<b>2.60 × 10</b>	1.06 × 10 <sup>2</sup>	9.02 × 10	9.48 × 10 <sup>5</sup>	2.74 × 10 <sup>5</sup>
	SCA	9.58 × 10 <sup>2</sup>	4.18 × 10 <sup>2</sup>	2.40 × 10 <sup>2</sup>	1.10 × 10 <sup>9</sup>	2.89 × 10 <sup>6</sup>
	IJAYA	1.38 × 10 <sup>2</sup>	2.30 × 10 <sup>2</sup>	1.18 × 10 <sup>2</sup>	6.54 × 10 <sup>6</sup>	3.06 × 10 <sup>5</sup>

### 7. Conclusions

The PV models’ parameters are located in the multi-modal and nonlinear solution space with various local optima so that it is extremely tricky for various existing MFO algorithms to extract a set of optimal parameters of the PV models. This paper proposes an improved MFO (IMFO) algorithm for estimating the parameters of PV models. In IMFO, the DFG strategy has been first developed to generate two different types of high-performance target flames for effectively searching the global optimal solution. To effectively tackle the global exploration and local exploitation, two different update strategies are developed. In addition, we develop a probability to select one of above two update strategies for each moth during the iterative process, which ensures the balance between the global exploration and local exploitation. Due to effectively combining the DFG strategy with the two update strategies, IMFO can effectively accurately and reliably identify the different PV models’ parameters.

In the future, IMFO will be adopted to settle multi-objective and constrained problems or economic dispatch issues in power systems. Furthermore, some other improvements will be proposed to expand the use of complex renewable energy algorithms by optimization algorithms.

**Author Contributions:** Conceptualization, H.S., C.L., and Z.Y.; Methodology, H.S., C.L., Y.X., and Q.K.; Software, H.S., C.L., H.W., and Z.C.; Writing—Original draft preparation, H.S. and C.L.; Writing—Review and editing, H.S. and C.L.

**Funding:** This work was supported by the National Natural Science Foundation of China under Grants 61503177, 81660299, and 61863028, by the China Scholarship Council under the State Scholarship Fund (CSC No. 201606825041), by the Science and Technology Department of Jiangxi Province of China under Grants 20161ACB21007, 20171BBE50071, and 20171BAB202033, and by the Education Department of Jiangxi province of China under Grants GJJ14228 and GJJ150197.

**Conflicts of Interest:** The authors declare no conflict of interest.

### Appendix A

**Table A1.** Parameters settings of the compared algorithms.

Algorithm	Parameters
MFO	NP = 50
OMFO	NP = 40
WCMFO	NP = 40, $N_{sr} = 4$ , $N_{stream} = N_{pop} - N_{sr}$ , $\beta = 3/2$
BSO	NP = 50, $p_{r0} = 0.2$ , $p_{r1} = 0.8$ , $p_{r11} = 0.4$ , $p_{r21} = 0.5$ , $c = 25$ , $M = 5$
CLPSO	NP = 40, $w = 0.9-0.2$ , $c = 1.49445$ , $m = 5$
ABC	NP = 50, $\alpha = 1$ , $limit = 100$
SCA	NP = 50
IJAYA	NP = 50
IMFO	NP = 100, $m = 4$ , $P = 0.4$

**Table A2.** Absolute error of IMFO for each measured on the single diode model.

Item	$V_{\text{measured}}(\text{V})$	$I_{\text{measured}}(\text{A})$	$I_{\text{simulated}}(\text{A})$	IAE
1	-0.2057	0.7640	0.76408801	0.00008801
2	-0.1291	0.7620	0.76266328	0.00066328
3	-0.0588	0.7605	0.76135541	0.00085541
4	0.0057	0.7605	0.76015400	0.00034600
5	0.0646	0.7600	0.75905514	0.00094486
6	0.1185	0.7590	0.75804220	0.00095780
7	0.1678	0.7570	0.75709145	0.00009145
8	0.2132	0.7570	0.75614111	0.00085889
9	0.2545	0.7555	0.75508658	0.00041342
10	0.2924	0.7540	0.75366357	0.00033643
11	0.3269	0.7505	0.75139069	0.00089069
12	0.3585	0.7465	0.74735365	0.00085365
13	0.3873	0.7385	0.74011717	0.00161717
14	0.4137	0.7280	0.72738237	0.00061763
15	0.4373	0.7065	0.70697301	0.00047301
16	0.4590	0.6755	0.67528069	0.00021931
17	0.4784	0.6320	0.63075889	0.00124111
18	0.4960	0.5730	0.57192892	0.00107108
19	0.5119	0.4990	0.49960738	0.00060738
20	0.5265	0.4130	0.41364884	0.00064884
21	0.5398	0.3165	0.31750984	0.00100984
22	0.5521	0.2120	0.21215441	0.00015441
23	0.5633	0.1035	0.10225068	0.00124932
24	0.5736	-0.0100	-0.00871799	0.00128201
25	0.5833	-0.1230	-0.12550748	0.00250748
26	0.5900	-0.2100	-0.20847181	0.00152819

**Table A3.** Absolute error of IMFO for each measured on the double diode model.

Item	$V_{\text{measured}}(\text{V})$	$I_{\text{measured}}(\text{A})$	$I_{\text{simulated}}(\text{A})$	IAE
1	-0.2057	0.7640	0.76399414	0.00000586
2	-0.1291	0.7620	0.76261019	0.00061019
3	-0.0588	0.7605	0.76133957	0.00083957
4	0.0057	0.7605	0.76017183	0.00032817
5	0.0646	0.7600	0.75910236	0.00089764
6	0.1185	0.7590	0.75811332	0.00088668
7	0.1678	0.7570	0.75717857	0.00017857
8	0.2132	0.7570	0.75623282	0.00076718
9	0.2545	0.7555	0.75516740	0.00033260
10	0.2924	0.7540	0.75371531	0.00028469
11	0.3269	0.7505	0.75139682	0.00089682
12	0.3585	0.7465	0.74730504	0.00080504
13	0.3873	0.7385	0.74001983	0.00151983
14	0.4137	0.7280	0.72725956	0.00074044
15	0.4373	0.7065	0.70686255	0.00036255
16	0.4590	0.6755	0.67521858	0.00028142
17	0.4784	0.6320	0.63076237	0.00123763
18	0.4960	0.5730	0.57199017	0.00100983
19	0.5119	0.4990	0.49969784	0.00069784
20	0.5265	0.4130	0.41372571	0.00072571
21	0.5398	0.3165	0.31754180	0.00104180
22	0.5521	0.2120	0.21212422	0.00012422
23	0.5633	0.1035	0.10216958	0.00133042
24	0.5736	-0.0100	-0.00878600	0.00121400
25	0.5833	-0.1230	-0.12553982	0.00253982
26	0.5900	-0.2100	-0.20837881	0.00162119

**Table A4.** Absolute error of IMFO for each measured on the PV module model.

Item	$V_{\text{measured}}(\text{V})$	$I_{\text{measured}}(\text{A})$	$I_{\text{simulated}}(\text{A})$	IAE
1	0.1248	1.0315	1.02912657	0.00237343
2	1.8093	1.0300	1.02738585	0.00261415
3	3.3511	1.0260	1.02574421	0.00025579
4	4.7622	1.0220	1.02410747	0.00210747
5	6.0538	1.0180	1.02229035	0.00429035
6	7.2364	1.0155	1.01992786	0.00442786
7	8.3189	1.0140	1.01635944	0.00235944
8	9.3097	1.0100	1.01049231	0.00049231
9	10.2163	1.0035	1.00062569	0.00287431
10	11.0449	0.9880	0.98454637	0.00345363
11	11.8018	0.9630	0.95952145	0.00347855
12	12.4929	0.9255	0.92284049	0.00265951
13	13.1231	0.8725	0.87260289	0.00010289
14	13.6983	0.8075	0.80727824	0.00022176
15	14.2221	0.7265	0.72834029	0.00184029
16	14.6995	0.6345	0.63714077	0.00264077
17	15.1346	0.5345	0.53621417	0.00171417
18	15.5311	0.4275	0.42951068	0.00201068
19	15.8929	0.3185	0.31877223	0.00027223
20	16.2229	0.2085	0.20738624	0.00111376
21	16.5241	0.1010	0.09616350	0.00483650
22	16.7987	-0.0080	-0.00832793	0.00032793
23	17.0499	-0.1110	-0.11093729	0.00006271
24	17.2793	-0.2090	-0.20924554	0.00024554
25	17.4885	-0.3030	-0.30085833	0.00214167

**Table A5.** CEC2017 benchmark functions with initialization and search range:  $(-100,100)^D$ .

Types	No.	Functions	$F[x^*]$
Unimodal	F1	Shifted and Rotated Bent Cigar Instance	100
	F2	Shifted and Rotated Sum of Different Power Instance	200
	F3	Shifted and Rotated Zakharov Instance	300
Multimodal	F4	Shifted and Rotated Rosenbrock's Instance	400
	F5	Shifted and Rotated Rastrigin's Instance	500
	F6	Shifted and Rotated Expanded Scaffer's F6 Instance	600
	F7	Shifted and Rotated Lunacek Bi_Rastrigin Instance	700
	F8	Shifted and Rotated Non-Continuous Rastrigin's Instance	800
	F9	Shifted and Rotated Levy Instance	900
	F10	Shifted and Rotated Schwefel's Instance	1000
Hybrid	F11	Hybrid Instance 1 (N = 3)	1100
	F12	Hybrid Instance 2 (N = 3)	1200
	F13	Hybrid Instance 3 (N = 3)	1300
	F14	Hybrid Instance 4 (N = 4)	1400
	F15	Hybrid Instance 5 (N = 4)	1500
	F16	Hybrid Instance 6 (N = 4)	1600
	F17	Hybrid Instance 6 (N = 5)	1700
	F18	Hybrid Instance 6 (N = 5)	1800
	F19	Hybrid Instance 6 (N = 5)	1900
	F20	Hybrid Instance 6 (N = 6)	2000
Composition	F21	Composition Instance 1 (N = 3)	2100
	F22	Composition Instance 2 (N = 3)	2200
	F23	Composition Instance 3 (N = 4)	2300
	F24	Composition Instance 4 (N = 4)	2400
	F25	Composition Instance 5 (N = 5)	2500
	F26	Composition Instance 6 (N = 5)	2600
	F27	Composition Instance 7 (N = 6)	2700
	F28	Composition Instance 8 (N = 6)	2800
	F29	Composition Instance 9 (N = 3)	2900
	F30	Composition Instance 10 (N = 3)	3000

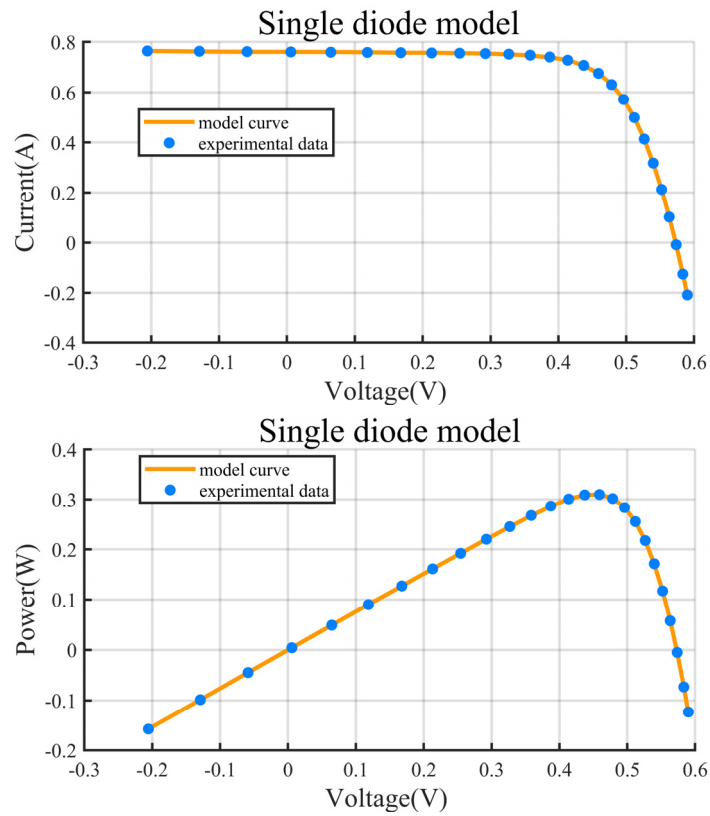


**Figure A1.** Comparisons between the experimental data and simulated data obtained by IMFO for single diode model:  $I$ - $V$  and  $P$ - $V$  characteristics.

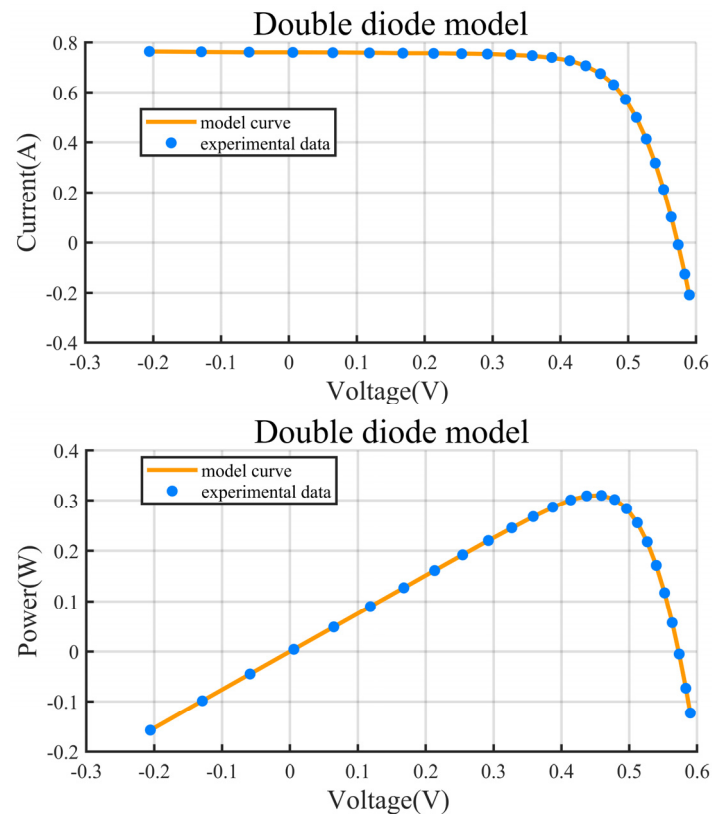


**Figure A2.** Comparisons between the experimental data and simulated data obtained by IMFO for double diode model:  $I$ - $V$  and  $P$ - $V$  characteristics.

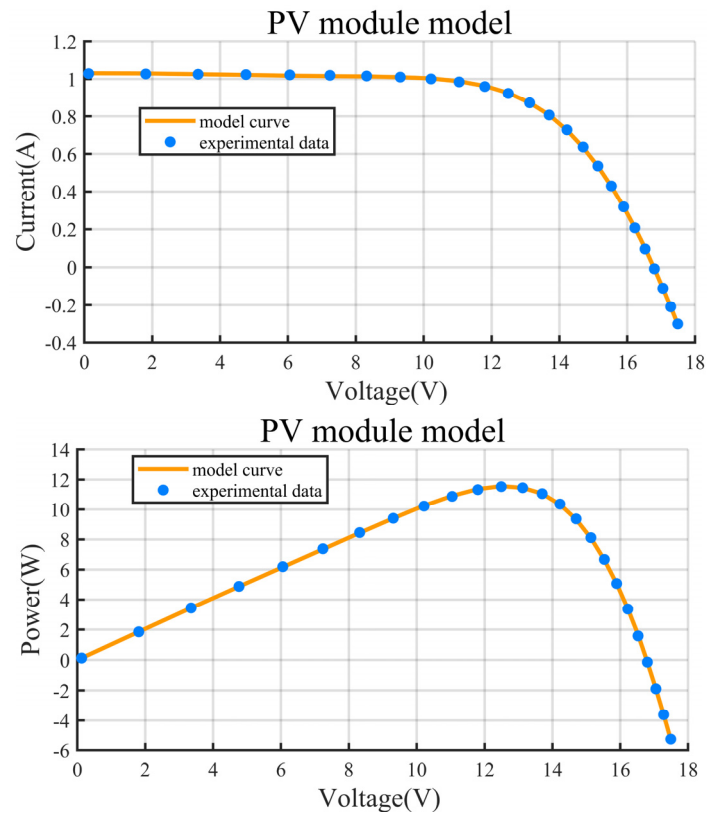


**Figure A3.** Comparisons between the experimental data and simulated data obtained by IMFO for PV module model: *I-V* and *P-V* characteristics.

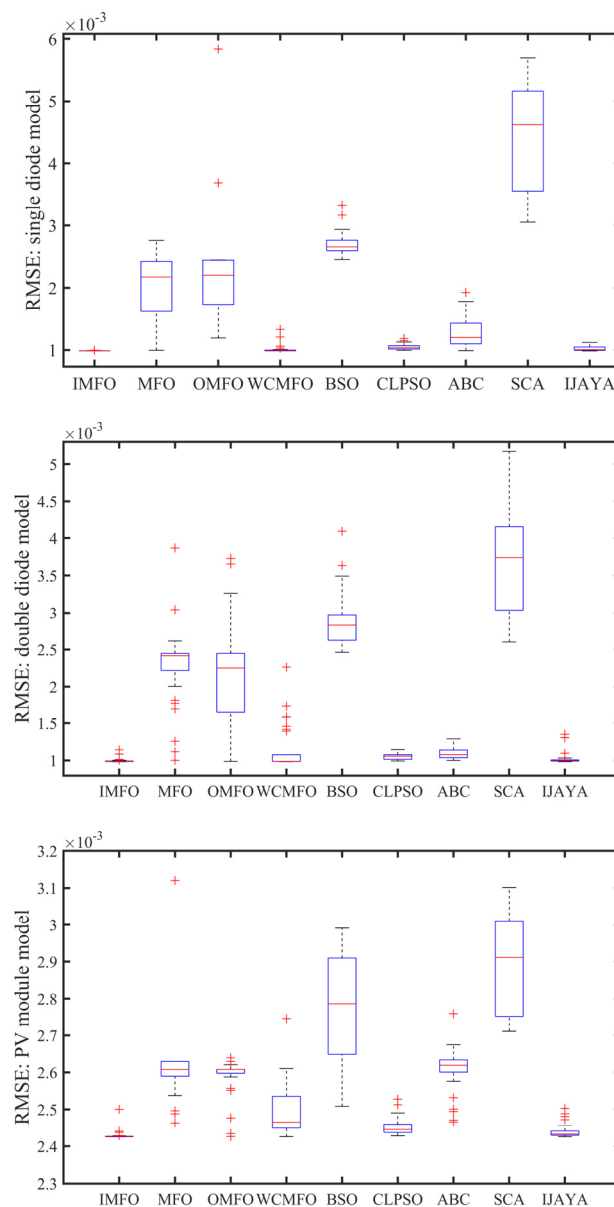


**Figure A4.** Best RMSE boxplot over 30 runs of different algorithms for three models.

## References

1. Awan, A.B.; Khan, Z.A. Recent progress in renewable energy—Remedy of energy crisis in Pakistan. *Renew. Sustain. Energy Rev.* **2014**, *33*, 236–253. [[CrossRef](#)]
2. Irmak, E.; Ayaz, M.S.; Gok, S.G.; Sahin, A.B. A survey on public awareness towards renewable energy in Turkey. In Proceedings of the 2014 International Conference on Renewable Energy Research and Application (ICRERA), Milwaukee, WI, USA, 19–22 October 2014; pp. 932–937.
3. Jha, S.K.; Bilalovic, J.; Jha, A.; Patel, N.; Zhang, H. Renewable energy: Present research and future scope of Artificial Intelligence. *Renew. Sustain. Energy Rev.* **2017**, *77*, 297–317. [[CrossRef](#)]
4. Lau, L.C.; Lee, K.T.; Mohamed, A.R. Global warming mitigation and renewable energy policy development from the Kyoto Protocol to the Copenhagen Accord—A comment. *Renew. Sustain. Energy Rev.* **2012**, *16*, 5280–5284. [[CrossRef](#)]
5. Mcelroy, M.B.; Chen, X. Wind and Solar Power in the United States: Status and Prospects. *CSEE J. Power Energy Syst.* **2017**, *3*, 1–6. [[CrossRef](#)]

6. Hanger, S.; Komendantova, N.; Schinke, B.; Zejli, D.; Ihlal, A.; Patt, A. Community acceptance of large-scale solar energy installations in developing countries: Evidence from Morocco. *Energy Res. Soc. Sci.* **2016**, *14*, 80–89. [[CrossRef](#)]
7. Abbassi, R.; Chebbi, S. Energy management strategy for a grid-connected wind-solar hybrid system with battery storage: Policy for optimizing conventional energy generation. *Int. Rev. Electr. Eng.* **2012**, *7*, 3979–3990.
8. Wu, Z.; Tazvinga, H.; Xia, X. Demand side management of photovoltaic-battery hybrid system. *Appl. Energy* **2015**, *148*, 294–304. [[CrossRef](#)]
9. Chen, Z.; Wu, L.; Lin, P.; Wu, Y.; Cheng, S.; Yan, J. Parameters identification of photovoltaic models using hybrid adaptive Nelder-Mead simplex algorithm based on eagle strategy. *Appl. Energy* **2016**, *182*, 47–57. [[CrossRef](#)]
10. Fathy, A.; Rezk, H. Parameter estimation of photovoltaic system using imperialist competitive algorithm. *Renew. Energy* **2017**, *111*, 307–320. [[CrossRef](#)]
11. Askarzadeh, A.; Rezaazadeh, A. Parameter identification for solar cell models using harmony search-based algorithms. *Sol. Energy* **2012**, *86*, 3241–3249. [[CrossRef](#)]
12. Chan, D.S.H.; Phang, J.C.H. Analytical methods for the extraction of solar-cell single and double-diode model parameters from I–V characteristics. *IEEE Trans. Electron. Devices* **1987**, *34*, 286–293. [[CrossRef](#)]
13. Tong, N.T.; Kamolpattana, K.; Pora, W. A deterministic method for searching the maximum power point of a PV panel. In Proceedings of the International Conference on Electrical Engineering/Electronics, Computer, Telecommunications and Information Technology, Hua Hin, Thailand, 24–27 June 2015; pp. 1–6.
14. Bastidasrodriguez, J.D.; Petrone, G.; Ramospaja, C.A.; Spagnuolo, G. A genetic algorithm for identifying the single diode model parameters of a photovoltaic panel. *Math. Comput. Simul.* **2017**, *131*, 38–54. [[CrossRef](#)]
15. Ma, J.; Ting, T.O.; Man, K.L.; Zhang, N.; Guan, S.U.; Wong, P.W.H. Parameter estimation of photovoltaic models via cuckoo search. *J. Appl. Math.* **2013**, *2013*, 1–11. [[CrossRef](#)]
16. Ortiz-Conde, A.; Sánchez, F.J.G.; Muci, J. New method to extract the model parameters of solar cells from the explicit analytic solutions of their illuminated characteristics. *Sol. Energy Mater. Sol. Cells* **2006**, *90*, 352–361. [[CrossRef](#)]
17. Saleem, H.; Karmalkar, S. An analytical method to extract the physical parameters of a solar cell from four points on the illuminated j–v curve. *IEEE Electron Device Lett.* **2009**, *30*, 349–352. [[CrossRef](#)]
18. Easwarakhanthan, T.; Bottin, J.; Bouhouch, I.; Boutrit, C. Nonlinear minimization algorithm for determining the solar cell parameters with microcomputers. *Int. J. Sol. Energy* **1986**, *4*, 1–12. [[CrossRef](#)]
19. Soon, J.J.; Low, K.S. Photovoltaic model identification using particle swarm optimization with inverse barrier constraint. *IEEE Trans. Power Electron.* **2012**, *27*, 3975–3983. [[CrossRef](#)]
20. Oliva, D.; Cuevas, E.; Pajares, G. Parameter identification of solar cells using artificial bee colony optimization. *Energy* **2014**, *72*, 93–102. [[CrossRef](#)]
21. Jiang, L.L.; Maskell, D.L.; Patra, J.C. Parameter estimation of solar cells and modules using an improved adaptive differential evolution algorithm. *Appl. Energy* **2013**, *112*, 185–193. [[CrossRef](#)]
22. Askarzadeh, A.; Rezaazadeh, A. Extraction of maximum power point in solar cells using bird mating optimizer-based parameters identification approach. *Sol. Energy* **2013**, *90*, 123–133. [[CrossRef](#)]
23. Oliva, D.; El Aziz, M.A.; Hassanien, A.E. Parameter estimation of photovoltaic cells using an improved chaotic whale optimization algorithm. *Appl. Energy* **2017**, *200*, 141–154. [[CrossRef](#)]
24. Wu, Z.; Yu, D.; Kang, X. Parameter identification of photovoltaic cell model based on improved ant lion optimizer. *Energy Convers. Manag.* **2017**, *151*, 107–115. [[CrossRef](#)]
25. Rajasekar, N.; Kumar, N.K.; Venugopalan, R. Bacterial Foraging Algorithm based solar PV parameter estimation. *Sol. Energy* **2013**, *97*, 255–265. [[CrossRef](#)]
26. Yu, K.; Liang, J.; Qu, B.; Chen, X.; Wang, H. Parameters identification of photovoltaic models using an improved JAYA optimization algorithm. *Energy Convers. Manag.* **2017**, *150*, 742–753. [[CrossRef](#)]
27. Patel, S.J.; Panchal, A.K.; Kheraj, V. Extraction of solar cell parameters from a single current–voltage characteristic using teaching-learning-based optimization algorithm. *Appl. Energy* **2014**, *119*, 384–393. [[CrossRef](#)]
28. Alam, D.F.; Yousri, D.A.; Eteiba, M.B. Flower Pollination Algorithm based solar PV parameter estimation. *Energy Convers. Manag.* **2015**, *101*, 410–422. [[CrossRef](#)]

29. Mirjalili, S. Moth-flame optimization algorithm: A novel nature-inspired heuristic paradigm. *Knowl.-Based Syst.* **2015**, *89*, 228–249. [[CrossRef](#)]
30. Allam, D.; Yousri, D.A.; Eteiba, M.B. Parameters extraction of the three diode models for the multi-crystalline solar cell/module using Moth-Flame Optimization Algorithm. *Energy Convers. Manag.* **2016**, *123*, 535–548. [[CrossRef](#)]
31. Aghaie, R.; Farshad, M. Maximum Power Point Tracker for Photovoltaic Systems Based on Moth-Flame Optimization Considering Partial Shading Conditions. *J. Oper. Autom. Power Eng.* **2019**. [[CrossRef](#)]
32. Aouchiche, N.; Aitcheikh, M.S.; Becherif, M.; Ebrahim, M.A. AI-based global MPPT for partial shaded grid connected PV plant via MFO approach. *Sol. Energy* **2018**, *171*, 593–603. [[CrossRef](#)]
33. Apinantanakon, W.; Sunat, K. OMFO: A New Opposition-Based Moth-Flame Optimization Algorithm for Solving Unconstrained Optimization Problems. Recent Advances in Information and Communication Technology 2017, IC2IT 2017; In *Advances in Intelligent Systems and Computing*; Springer: Cham, Switzerland, 2017; Volume 566, pp. 22–31.
34. Khalilpourazari, S.; Khalilpourazary, S. An efficient hybrid algorithm based on Water Cycle and Moth-Flame Optimization algorithms for solving numerical and constrained engineering optimization problems. *Soft Comput.* **2019**, *2013*, 1–24. [[CrossRef](#)]
35. Wu, W.-M.; Li, Z.-X.; Lin, Z.-Y.; Wu, W.-Y.; Fang, D.-Y. Moth-flame optimization algorithm based on chaotic crisscross operator. *J. Comput. Eng. Appl.* **2018**, *54*, 136–141.
36. Wolf, M.; Noel, G.T.; Stirn, R.J. Investigation of the double exponential in the current–voltage characteristics of silicon solar cells. *Electron Devices IEEE Trans.* **1977**, *24*, 419–428. [[CrossRef](#)]
37. Alrashidi, M.R.; Alhajri, M.F.; Elnaggar, K.M.; Alothman, A.K. A new estimation approach for determining the i–v characteristics of solar cells. *Sol. Energy* **2011**, *85*, 1543–1550. [[CrossRef](#)]
38. Niu, Q.; Zhang, H.; Li, K. An improved TLBO with elite strategy for parameters identification of PEM fuel cell and solar cell models. *Int. J. Hydrogen Energy* **2014**, *39*, 3837–3854. [[CrossRef](#)]
39. Chen, X.; Yu, K.; Du, W.; Zhao, W.; Liu, G. Parameters identification of solar cell models using generalized oppositional teaching learning-based optimization. *Energy* **2016**, *99*, 170–180. [[CrossRef](#)]
40. Shi, Y. Brain storm optimization algorithm. In *International Conference on Swarm Intelligence*; Springer: Berlin/Heidelberg, Germany, 2011; pp. 303–309.
41. Liang, J.J.; Qin, A.K.; Suganthan, P.N.; Baskar, S. Comprehensive learning particle swarm optimizer for global optimization of multimodal functions. *IEEE Trans. Evol. Comput.* **2006**, *10*, 281–295. [[CrossRef](#)]
42. Mirjalili, S. SCA: A Sine Cosine Algorithm for solving optimization problems. *Knowl.-Based Syst.* **2016**, *96*, 120–133. [[CrossRef](#)]
43. Alcalá-Fdez, J.; Sanchez, L.; Garcia, S.; del Jesus, M.J.; Ventura, S.; Garrell, J.; Otero, J.; Romero, C.; Bacardit, J.; Rivas, V.M.; et al. KEEL: A software tool to assess evolutionary algorithms for data mining problems. *Soft Comput.* **2009**, *13*, 307–318. [[CrossRef](#)]
44. Awad, N.; Ali, M.; Liang, J.; Qu, B.; Suganthan, P. *Problem Definitions and Evaluation Criteria for the CEC2017 Special Session and Competition on Single Objective Real-Parameter Numerical Optimization*; Technical Report; NTU: Singapore, 2016.

